A Short-Term Energy Management of Microgrids Considering Renewable Energy Resources, Micro-Compressed Air Energy Storage and DRPs

Leila Bagherzadeh[1], Hossein Shahinzadeh[2]‡, Hossein Shayeghi[1], Gevork B. Gharehpetian[2]

1- Department of Electrical Engineering, University of Mohaghegh Ardabili, Ardabil, Iran

2- Department of Electrical Engineering, Amirkabir University of Technology (Tehran Polytechnic), Tehran, Iran

(bagherzadeh@student.uma.ac.ir, h.s.shahinzadeh@ieee.org, hshayeghi@uma.ac.ir, grptian@aut.ac.ir)

‡ Hossein Shahinzadeh; Corresponding Author, IEEE Member, Department of Electrical Engineering, Amirkabir University of Technology (Tehran Polytechnic), Tehran, Iran, Fax: +982166406469, Email: h.s.shahinzadeh@ieee.org

Received: 14.10.2019 Accepted:02.12.2019

Abstract- The extensive penetration of renewable resources and utilizing advanced energy management techniques as well as enabling demand response programs (DRPs), especially in microgrids and active distribution networks, has had an impressive impact on the operation of such grids. Thus, with respect to the active and influential role of distribution grids in the restructured environment and the objective of achieving optimal operation of microgrids, energy management in this new environment requires more comprehensive analytic studies and rigorous researches. In this regard, the present research proposes a new strategy of optimal energy management and the subsequent day-ahead scheduling of a microgrid in the presence of micro compressed air energy storage (MCAES) and considering the uncertainties of renewable energy resources. The minimization of operation costs of energy storage facilities, environmental emission, the costs corresponded with the energy not supplied (ENS) and excess generation capacity are the main objectives of this study while the load satisfaction constraints are imposed. The technical constraints of distributed generation resources and energy storage facilities are imposed on this optimization problem. Besides, the execution of demand-side management programs is modelled to flatten the demand curve and to close the operational condition on the most optimum point. Employing the teaching-learning-based optimization (TLBO) algorithm, the proposed method is simulated for a test microgrid. The simulation's results show that the utilization of MCAES facilities and executing DRPs have been concluded to the mitigation of generation cost, alleviation of emission, and reduction of ENS and excess generation capacity of the microgrid.

Keywords- Optimal energy management, Renewable energy resources, Environmental constraints, Energy storage, Demand response programs, Uncertainty.

1. Introduction

In some locations, where the expansion of the main power system is not technically or economically viable, the islanding microgrid scheme is suggested. According to the report issued by international energy agency [1], well above 1 billion people do not access to the electricity networks. In order to supply such loads, two options exist for power system planners and engineers. The first is the expansion of the transmission network, and the second is the execution of an isolated microgrid. Some obstacles, such as high prices of fuel and emission of greenhouse gases restrain the use of fossil fuels. Hence, the implementation of a renewable-oriented isolated microgrid is a proper solution for these restrictions. Solar and wind energy are highly dependent on weather condition that makes them have inevitable uncertainties. Hence, the utilization of an energy storage facility is indispensable. In [2], the economic and reliability concepts of the microgrids are investigated. In [3], the optimal placement of distributed generation (DG) resources is proposed, and suggested strategies are assessed. The increase of use of combined heat and power (CHP) DGs is also described in [4], in which it is objected to improving the reliability of microgrids. The short-term generation scheduling for microgrids is also evaluated in [5]. In [6], a multi-objective optimization is conducted to deal with the energy management of microgrids while the economic and environmental restrictions are taken into account. Some types of DG technologies such as internal combustion engines, gas turbines, micro-turbines, fuel cells, photovoltaic cells, and wind turbines have had immense pervasiveness due to tremendous technological growth as well as being eco-friendly [7]. Hence, the usage of fossil-based generators in distribution networks is not favoured economically and environmentally. The microgrid structure is an appropriate

platform for integration of DGs [8]. In [9], the considered microgrid consists of a set of loads and a set of small-scale resources as a controllable system, which provides thermal and electrical power for a specific region. In [10, 11], the benefits of a microgrid scheme, such as the increase in local reliability (load indices), reduction of power losses in supplying branch, local voltage improvement, and compensation of voltage drop are described. The microgrid is capable of operating in two modes of being connected to the upstream network or isolated [11]. The precise predictions indicate that 25% of total generation till 2040 will be provided by wind farms. In addition, 20% will be produced by chemical cells, and 30% will be generated by solar panels by 2040 [12]. A vast network is composed of several small grids, in which DGs are installed in the vicinity of loads. Such a structure enables the capability of extensive use of renewable energy resources [13]. The amount of electrical power generation by renewable resources depends on the ambient condition of the DG's installation location, such as solar radiation or wind speed. Thus, the intermittency of these resources necessitates the utilization of energy storage facilities to meet the demand. Batteries are the usual option to store electrical energy. However, they are unable to store electricity for long-term applications due to their small-scale storage capability and being crashed due to inactivity [14]. The compressed air energy storage facility is one of the emerging technologies which has assumed special importance in recent years [15-17]. In this scheme, the excess generated power during off-peak hours is being used to compress the air into a natural or artificial reservoir. The compressed air can be stored in natural salt caverns or metal tanks and must be expanded to drive a turbine connected to a combustion gas turbine when it is needed. Nowadays, in order to shift the peak power to the off-peak hours, which consequently leads to a flatter load profile, the demand response programs (DRPs) are widely designed [18]. One of the most prevalent kinds of DRPs is "time of use" [19]. This program causes the load shifting from peak hours to off-peak hours that makes the load profile flatter. During peak hours, due to high power consumption, renewable resources and the storage device may be unable to meet the demand, which can be led to an increase in the cost of energy not supplied. The consumers tend to change their consumption time to off-peak hours to reduce their energy costs [20]. This segregation can also be performed for the hours of a day, the days of a week, or seasons of a year. In [20], it is supposed that at each time interval, only 9% of the load can be shifted to other intervals. However, in our study, the maximum load shifting rate of 15% can be imposable. In this research, the novel strategy of use of micro compressed air energy storage (MCAES) with calling DRPs into the microgrid in islanding mode is investigated. This energy management strategy is designed based on the optimum contribution of generation resources as well as optimum charging/discharging rate of MCAES and battery facilities, which are categorized and evaluated through four scenarios. The first scenario is defined so that no renewable resources, no storage facility, and no DRP are integrated, and the whole demand must be supplied by micro-turbines. In the second scenario, renewable resources such as wind and solar energies are integrated. In the 3rd scenario, the impact of the presence of MCAES unit along with renewable energy resources is evaluated. Ultimately, in the 4th scenario, the renewable energy resources, the MCAES unit, the DRPs are integrated into the model to meet the loads. The micro-turbines are committed in all scenarios. The targeted objective function is made up of four goals of minimization of generation cost of storage devices, environmental emission, the costs associated with energy not supplied, and the costs correlated with excess generation capacity. The solution space of the optimization problem is also restricted by load satisfaction constraints, the technical limitations of distributed generation resources and energy storage facilities.

2. The modelling of Microgrid's component

The targeted microgrid in this paper contains wind turbines and photovoltaic cells. In addition, in order to ensure the continuous supply of loads, the battery storage unit is utilized. As the new strategy for energy management in the isolated microgrid, the MCAES facility is committed for provision of power while the elastic loads react against the price variation with respect to DRPs. Fig. 1 illustrates the paradigm of the targeted microgrid. In the following subcategories, the microgrid's components will be explained.

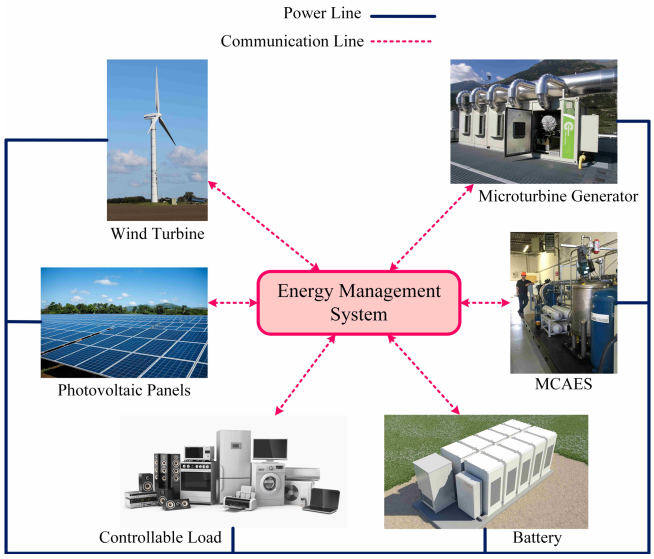

Fig. 1. The structure of the microgrid in islanding mode

2.1. Wind turbine and the modeling of wind speed uncertainty

The output power of the wind turbine variates corresponded with the wind velocity. The past studies such as [21-22] show that the wind speed curve in a specific region often follows the Weibull distribution. Hence, in this study, it is supposed accordingly. The forecasted wind speeds are described by their average values. The probability density function of the wind speed, which is characterized by Weibull distribution, is shown in Eq. (1):

$$f(v) = (k/c)\cdot(v/c)^{(k-1)} exp^{-(v/c)^k} \quad , \quad 0<v<\infty \qquad (1)$$

In the above equation, v, k, and c represent the wind velocity, the shape parameter (without dimension), and scale parameter, respectively. The truncation and segregation of the wind speed distribution records can simplify the problem. For each interval, the random variable of wind speed is normalized by the mean value of wind speed in Weibull

distribution. The truncation point can be enhanced from the mean value to the point where the overall coverage is achieved. After truncation, the distribution can be divided into separate parts, the quantity of which is corresponded with the desired accuracy. By integration, the probability of each part can be easily calculated. A 5-segment wind speed distribution is depicted in Fig. 2.

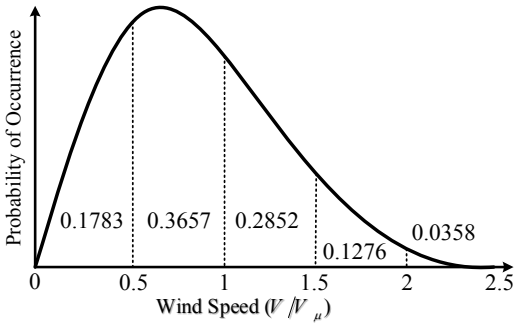

Fig. 2. The probability distribution of wind speed

By a specific wind speed distribution and a wind to power conversion function, the wind power distribution can be obtained. In this study, the power conversion function is defined as Eq. (2) as below [23]:

$$w=\begin{cases}0 & , \quad v<v_i \\ w_r(v-v_i)/(v_r-v_i) & , \quad v_i \le v \le v_r \\ w_r & , \quad v_r \le v \le v_o \\ 0 & , \quad v>v_o \end{cases} \tag{2}$$

Where, w, w_r, v_i, v_r, and v_o denote the output power of the wind turbine in kW, the relative power, the cut-in wind speed, the rated wind speed, and the cut-out wind speed, respectively.

2.2. The photovoltaic cell and the solar radiation uncertainty modeling

In fact, the output power of the photovoltaic system depends absolutely on solar radiation. The hourly solar radiation in a specific region can appropriately be modelled by a bi-exponential distribution as it is described in [24-26]. It can also be described as a linear function composed of two exponential functions stated in [27].

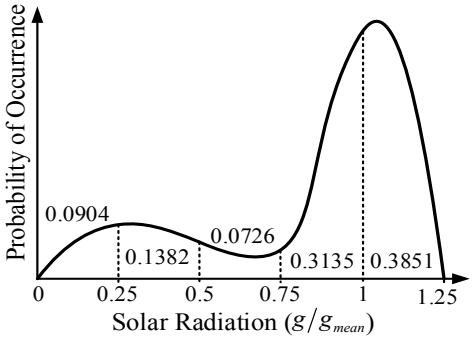

Fig. 3. The probability distribution of solar radiation

$$f(g)=w(k_1/c_1)\cdot(g/c_1)^{(k_1-1)}exp^{-(g/c_1)^{k_1}} +(1-w)\cdot(k_2/c_2)\cdot(g/c_2)^{(k_2-1)}exp^{-(g/c_2)^{k_2}} \quad , \quad 0<g<\infty \tag{3}$$

Where, g shows the radiation density in kW/m^2, w indicates on weighting factor, k denotes the shape parameter, and finally, c_1 and c_2 show the scale parameters. Similar to the wind speed distribution model, solar radiation distribution can also be truncated [28]. A solar radiation distribution is depicted in Fig. 3.

By a specific probability distribution of solar variation for a specific region along with the solar radiation to power conversion function, the distribution of photovoltaic power generation can be achieved. The employed conversion function in this study is figured out by Eq. (4) as below [29]:

$$p=\eta^{pv}\times s^{pv}\times g \tag{4}$$

Where p denotes the output power of the photovoltaic unit in kW, η^{pv} describes the efficiency percentage, and s^{pv} indicates the entire photovoltaic panel surface in m^2.

2.3. Micro-turbine

The micro-turbines are the small-scale combustion turbines, which can procure more efficiency by using the heat of exhausting gases in comparison with diesel generators. A micro-turbine is a fast-response generator that is capable of tracking the load variations within its maximum and minimum generation range. The micro-turbines are also regarded as quick-start units to be used as non-spinning reserve capacities. In the proposed model for micro-turbines, the fuel costs, operation, and maintenance cost and technical constraints are taken into account. The fuel cost of micro-turbines can be described by a quadratic function of output active power as it is shown in Eq. (5):

$$FC_t^{MT}=\sum_{G=1}^{N_{MT}}\left(f_{1G}+f_{2G}P_{G,t}^{MT}+f_{3G}(P_{G,t}^{MT})^2\right) \tag{5}$$

In the above equation, P_G^{MT} shows the output power of each micro-turbine, f_{1G}, f_{2G}, and f_{3G} are the constants relevant to the micro-turbine. The amount of exhausting gases of micro-turbine is proportional to fuel consumption [30, 31]. These emissions can be calculated by a quadratic function. In this study, the emission cost of the microgrid is neglected.

2.4. Battery model

Eqs. (6) to (14) represents the technical constraints of the battery unit [32-34]. Eq. (6) shows the initial energy stored in the battery. Eqs. (7) and (8) express the minimum and maximum storage levels of the battery. Besides, the maximum charging/discharging rates of the battery are defined by Eqs. (9) and (10). The operational limitations of battery storage are stated in Eqs. (11) and (12). This restriction is imposed by Eq. (13). Ultimately, the dynamic energy model of the battery at each time is shown by Eq. (14).

$$SOC_t^0=SOC_{initial} \tag{6}$$

$$SOC_t=SOC^{\max} \tag{7}$$

$$SOC_t\ge SOC^{\min} \tag{8}$$

$$P_t^{charge}\le P_{charge}^{\max}\times U_t^{charge} \tag{9}$$

$$P_t^{charge}\ge P_{charge}^{\min}\times U_t^{charge} \tag{10}$$

$$P_t^{disc}\le P_{disc}^{\max}\times U_t^{disc} \tag{11}$$

$$P_t^{disc}\ge P_{disc}^{\min}\times U_t^{disc} \tag{12}$$

$$U_t^{charge}+U_t^{disc}\le 1 \tag{13}$$

$$SOC_t=SOC_{t-1}+\eta_{ch}^B\times P_t^{charge}-\frac{P_t^{disc}}{\eta_{disc}^B} \tag{14}$$

In the above equations, SOC_t^0 is the energy of the battery at the beginning interval. $SOC_{initial}$ is the initial energy of battery. SOC^{max} and SOC^{min} represent the maximum and minimum energy of battery. P_{charge}^{max} and P_{charge}^{min} stand for the maximum and minimum power consumption rate while charging. P_{disc}^{max} and P_{disc}^{min} are the maximum and minimum discharge rates. η_{ch}^{B} and η_{disc}^{B} are the battery efficiency of charging and discharging. U_t^{charge} and U_t^{disc} stand for the binary variables of state of battery for charging and discharging. SOC_t is the state of charge of the battery at hour t. In addition, P_t^{charge} and P_t^{disc} show the power consumed or generated while charging or discharging processes at the interval of t.

2.5. Micro Compressed Air Energy Storage (MCAES) model

There is a fast-paced incremental interest in energy storage facilities due to the ever-growing penetration of intermittent renewable sources in both the supply-side and demand side. So far, some innovative emerging storage technologies are offered to cope with this stochastic nature of uncertain resources. However, compressed air energy storage (CAES) is regarded as one of the most practically viable and economically sensible solutions. A CAES system fundamentally resembles pumped-hydro energy storage facilities in terms of applications, storage capacity, and output. In a CAES scheme, the ambient air is the vehicle, in which the energy is stored during the compression process. Then, the compressed air is stored in underground salt caverns or small-scale aboveground facilities. The high-pressure air is expanded and heated toward a combustion turbine to generate electricity. Preferably, the storage unit owners and power system operators would like to store power during off-peak hours and deliver it to the grid back during peak hours to postpone the commitment of expensive units. When the storage of high volume of air in the underground reservoirs is not viable due to geological or economic reasons, the micro compressed air energy storage (MCAES) is a small-scale alternative, but over the earth's surface. The independence from the geological condition is an appealing feature of MCAES systems, which makes it viable to be installed wherever is more suitable from the technical point of view (e.g., in the vicinity of volatile wind farms or intermittent solar parks). MCAES facility has been usually used so far for maintaining uninterruptible power supply. High reliability, fast response capability, operational simplicity, reasonable generation cost, and high efficiency are the most salient characteristics of MCAES systems. Unlike a large-scale CAES scheme, in which compression is usually performed in two consecutive stages including intercooling, in an MCAES scheme, it is necessary to keep the structure simple and continuously and simultaneously achieve high-efficient performance. Hence, compression and expansion stages require to be closer to isothermal process than to adiabatic process. In an adiabatic-oriented CAES system, a vast amount of exergy is destructed due to a broad temperature difference between the beginning of the existing processes and the end of them, as well as a low recovery rate in the recuperator and hydraulic motor. In contrast, an isothermal process minimizes exergy losses and procure the opportunity to fulfil the desired temperatures after compression and expansion processes through mass flow regulation in order to satisfy the thermal loads. Therefore, the isothermal MCAES scheme is more efficient compared to other MCAES schemes and can be utilized in decentralized energy networks. In order to achieve a quasi-isothermal compression process, a large amount of water (or some other liquids) can be injected in the compressor to absorb the dissipating heat. Then the air-water (gas-liquid) mixture must be separated, and the stream of air must be cooled down to reach ambient temperature. Then the air is led to the storage tank. In parallel, by enjoying a hydraulic motor, the energy recovery practice from high-pressure water is done. Similarly, the water stream must be cooled down to be prepared for recirculation. In the expansion process, unlike the conventional CAES scheme, the air stream preheating measure in a combustion chamber or in a heat exchanger before entering into the turbine is not required. In the expansion stage, the exhausted air at the outlet of the turbine can be utilized to meet cooling loads in MCAES scheme. A quasi-isothermal compression process or expansion process can be regarded as a polytropic process model as can be shown in Eq. (15). The change of gas temperature during a polytropic process is given in Eq. (16):

$$Pv^n = Constant \tag{15}$$

$$\frac{T_{out}}{T_{in}} = \left[\frac{P_{out}}{P_{in}}\right]^{\frac{n-1}{n}} \tag{16}$$

In a quasi-isothermal compression process or expansion process, the change in the polytropic index n can give the possibility of control of mass flow rate for the injected liquid (especially water) that this matter makes it viable to match the temperature after compression stage to the heating temperature needed or the temperature after expansion stage to the cooling temperature needed. Hence, the ideal compression work ($w^{+}_{c,ideal}$) and expansion work ($w^{-}_{c,ideal}$) can be defined as follows. Besides, r shows the specific gas constant.

$$w^{+}_{c,ideal} = \left(\frac{rn}{n-1}\right)T_{out} - T_{in} \tag{17}$$

$$w^{-}_{e,ideal} = \left(\frac{rn}{n-1}\right)T_{in} - T_{out} \tag{18}$$

Therefore, isentropic efficiency (η_c, η_e) can be expressed as Eqs. (19) and (20), where w_c^{+} and w_e^{-} stand for actual compression and expansion work values.

$$\eta_c \equiv \frac{w^{+}_{c,ideal}}{w^{+}_{c}} \tag{19}$$

$$\eta_e \equiv \frac{w^{-}_{e}}{w^{-}_{e,ideal}} \tag{20}$$

The heat transfer rate from the gas state to the liquid state during compression (Q^{-}_c) and from the liquid to the gas state during the expansion process (Q^{+}_c) can be calculated by the following equations in kJ. In addition, h_{in} and h_{out} represent the specific enthalpy of input and output fluid, respectively, in kJ/kg, and M_a stands for the mass of flow of air.

$$Q^{-}_{c} = M_a\left[w^{+}_{c} - \left(h_{out} - h_{in}\right)\right] \tag{21}$$

$$Q^{+}_{e} = M_a\left[w^{+}_{e} - \left(h_{in} - h_{out}\right)\right] \tag{22}$$

In order to assess the energy efficiency, the following equations can be adopted. Eq. (23) indicate the storage efficiency, in which η_p is the baseload efficiency of the charging plant and Q represents the lower Calorific value. E_{in} and E_{out} are electric power input and output in kJ. The term $Q\eta_p$ expresses the electric energy that would be generated if the corresponding fuel consumed in MCAES is burned in another plant. Eq. (24) delineates the heating performance of the MCAES scheme considering the dissipated heat of the compression process. In this equation, Q_{hc} stands for the total compression's dissipated heat that is composed of summation of dissipated heat during compression (Q_c) and after compression (Q_{ac}). In order to assess cooling performance, without any fuel usage, Eq. (25) is defined, so that heat extraction from the ambient air for MCAES system is taken into consideration. In this equation, Q_{ce} stands for total extraction of heat from the source of the ambient air that is made up of two components of extracted heat during the expansion process (Q_e), and heat extraction after expansion process (Q_{ae}). The overall thermal efficiency can be expressed as Eq. (26). Fig. 4 portrays a general schematic overview of MCAES system.

$$\eta_s \equiv \frac{E_{out} - Q\eta_p}{E_{in}} \tag{23}$$

$$\eta_H \equiv \frac{Q_{hc}}{E_{in}} = \frac{Q_c + Q_{ac}}{E_{in}} \tag{24}$$

$$\eta_C \equiv \frac{Q_{ce}}{E_{in}} = \frac{Q_e + Q_{ae}}{E_{in}} \tag{25}$$

$$\eta_{th} \equiv \frac{E_{out} - E_{in}}{Q} \tag{26}$$

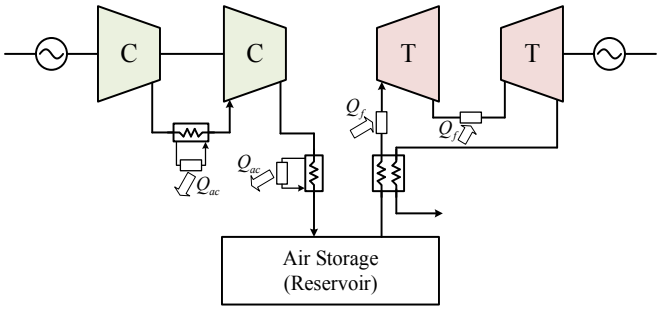

Fig. 4. The schematic of a two-stage MCAES system

In addition, by the employment of the following equations, the exergy of the quasi-isothermal MCAES model can be addressed as follows. Eq. (27) shows the general exergy balance, in which $\dot{E}^+$ and $\dot{E}^-$ show the exergy transfer rate to and from the system by work, heat, and mass in kW, and the exergy destruction is shown by $\dot{L}$ in kW. The exergy transfer rate to the system by the source of heat (E^+_q) is shown in Eq. (28). T stands for temperature in K. The exergy transfer rates, to and from the system, by the source of mass (E^+_y, E^-_y) are defined as (29), where k shows the specific flow exergy in kJ/kg, and s indicates the specific entropy in kJ/(kgK).

$$\dot{E}^+ - \dot{E}^- = \dot{L} \tag{27}$$

$$\dot{E}^+_q = \int \left(1 - \frac{T_0}{T}\right) \delta \dot{Q}^+ \tag{28}$$

$$\begin{cases} \dot{E}^+_{yk} \equiv \dot{M}_k \left(k_{in} - k_{out}\right) = \dot{M}_k \left[\left(h_{in} - h_{out}\right) - T_0 \left(s_{in} - s_{out}\right)\right] \\ \dot{E}^-_{yk} \equiv \dot{M}_k \left(k_{out} - k_{in}\right) = \dot{M}_k \left[\left(h_{out} - h_{in}\right) - T_0 \left(s_{out} - s_{in}\right)\right] \end{cases} \tag{29}$$

For the flow of air (gas flow), Eq. (30) can be presented. In this equation, P stands for pressure, and c_p is the specific heat.

$$\begin{cases} \left(h_{in} - h_{out}\right) = c_p \left(T_{in} - T_{out}\right) \\ \left(s_{in} - s_{out}\right) = c_p \ln \dfrac{T_{in}}{T_{out}} - r \ln \dfrac{P_{in}}{P_{out}} \end{cases} \tag{30}$$

In the case of the flow of liquid, Eq. (31) can be used instead, and the volumetric changes can be neglected.

$$\begin{cases} \left(h_{in} - h_{out}\right) = c\left(T_{in} - T_{out}\right) + \dfrac{P_{in} - P_{out}}{\rho} \\ \left(s_{in} - s_{out}\right) = c \ln \dfrac{T_{in}}{T_{out}} \end{cases} \tag{31}$$

In the case of the gas-liquid compression process, the exergy balance can be modified as Eq. (32). In below, E^-_{ya} and E^-_{yl} are the exergy transfer from the system by the flows of air and liquid.

$$\begin{cases} \dot{L}_c = \dot{E}^+ - \dot{E}^- \\ \dot{E}^+ = \dot{E}^+_c \\ \dot{E}^- = \dot{E}^-_{ya} + \dot{E}^-_{yl} \end{cases} \tag{32}$$

Thus, the exergy efficiency of the compression process can be defined as below with respect to the Second Law efficiency. In a similar way, the exergy efficiency of the expansion process can be formulated as Eq. (34).

$$\eta_{II,c} = \frac{\dot{E}^-}{\dot{E}^+} = \frac{\dot{E}^-_{ya} + \dot{E}^-_{yl}}{\dot{E}^+_c} \tag{33}$$

$$\eta_{II,e} = \frac{\dot{E}^-}{\dot{E}^+} = \frac{\dot{E}^-_e}{\dot{E}^+_{ya} + \dot{E}^+_{yl}} \tag{34}$$

The overall exergy efficiency of the entire MCAES system with a quasi-isothermal process can be expressed as follows [35-36]:

$$\eta_{II,MCAES} = \frac{\dot{E}^-}{\dot{E}^+} = \frac{\dot{E}^-_e + \dot{E}^-_{yl,c} + \dot{E}^-_{yl,ac} + \dot{E}^-_{yl,e} + \dot{E}^-_{yl,ae}}{\dot{E}^+_c} \tag{35}$$

2.6. Demand response model

In this paper, the employed DRP is a kind of time of use. The goal is to smooth the load curve by shifting the peak load to off-peak and mid-peak hours, which can be led to a decrease in the operation cost of the power system. The time-of-use program can be modeled as demonstrated in Fig. 5.

According to Fig. 5, and with respect to the selected DRP, only a certain part of the loads can be shifted to other periods by consumers. The mathematical formation of this concept is represented in Eqs. (36) and (37), which is shown below [37]:

$$Load^{DR}(t) = (1 - DR(t)) \times Load^{D}(t) + ldr(t) \tag{36}$$

$$Load^{D}(t) - Load^{DR}(t) = DR(t) \times Load^{D}(t) - ldr(t) \tag{37}$$

The technical constraints pertaining to DRP is mentioned in Eqs. (38) to (41). Eq. (38) indicates that the load is not increased or decreased rather than it is shifted from an hour to another. In other words, the decreasing load must be

equivalent to the increasing load in other periods, and the summation of each one must be exactly the same for the entire time horizon. The increasing load must be lower than a certain percentage of the baseload that is imposed by Eq. (39). Finally, the percentage of load reduction or increase must be lower than a certain amount that is specified by Eq. (40) and (41). This percentage is assumed to be 15% in this study.

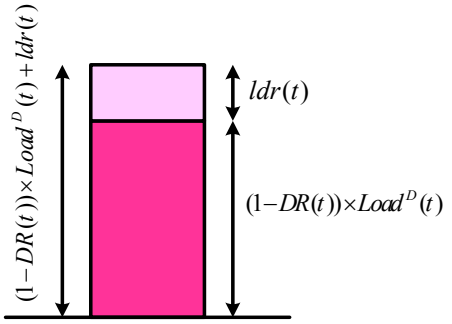

Fig. 5. The load's model regard to DRP

$$\sum_{t=1}^{T} ldr(t) = \sum_{t=1}^{T} DR(t) \times Load^D(t) \quad (38)$$

$$0 \le load^{inc}(t) \le inc(t) \times load^D(t) \quad (39)$$

$$DR(t) \le DR_{\max} \quad (40)$$

$$inc(t) \le inc_{\max} \quad (41)$$

In the above, $Load^D(t)$ represents the forecasted demand at hour t, DR_{max} and inc_{max} are the maximum percentages of load that can be reduced or increased. $ldr(t)$ is the load reduction rate. $Load^{inc}(t)$ is the maximum increasable load. $inc(t)$ is the percentage of maximum increasable load. $Load^{DR}(t)$ is the load with consideration of demand response programs. In addition, $DR(t)$ represents the amount of load reduction.

2.7. The energy not supplied and surplus power models

In a microgrid, which is operating in islanding mode, the outage of load or supply can be occurred planned or unplanned, which is inevitable. The former is known as load shedding, and the latter is known as curtailment. These two planned outages are applied to maintain the power balance constraint. If the momentary load is higher than the capacity of the summation of renewable energy resources and deliverable power storage unit, the grid is not able to satisfy the entire load, and it is necessary to impose load shedding. On the contrary, if the total load of the microgrid can be supplied by renewable resources, and if the storage units are fully charged, the excess generation of renewable resources must be curtailed. The unsupplied load is denoted by $P_{UN,t}$ and excess generation of renewable resources are shown by $P_{EX,t}$ [38-39].

3. The objective function and the problem's constraints

In this study, the main purpose of the new scheme of energy management is to obtain the optimum operation schedule of storage units (battery and MCAES) subject to minimize the operation cost of the microgrid. In the following parts, at first, the generation cost of storage units is explained. Then the suggested objective function along with the necessary constraints to solve the problem by teaching-learning-based optimization (TLBO) algorithm, are introduced.

3.1. The generation cost

The generation costs that a microgrid may be encountered with can be classified into three main categories of fuel cost, start-up cost, and the costs pertaining to power exchange with the upstream network. In the present work, in order to minimize the total generation cost, the following equations are contemplated.

$$\begin{aligned} Cost_{OP} &= Price_W \times P_W + Price_{PV} \times P_{PV} + Price_{MT} \times P_{MT} \\ &\pm Price_{MCAES} \times P_{MCAES} \pm Price_{Batt} \times P_{Batt} \pm Price_{Market} \times P_{Market} \end{aligned} \quad (42)$$

$$f_1 = Min \sum_{t=1}^{N_t} \mathrm{Cos}\, t_{OP}^t \quad (43)$$

In the above-mentioned equations, P_W, P_{MT}, P_{PV}, P_{Batt}, P_{MCAES}, and P_{Grid} stand for the generated active power by wind turbine, micro-turbine, photovoltaic panel, battery storage unit, MCAES unit, and the amount of exchanged power with the power market in kW respectively. In addition, N_t represents the total number of intervals within the targeted operation time horizon. Moreover, $Price_W$, $Price_{MT}$, $Price_{PV}$, $Price_{Batt}$, $Price_{MCAES}$, and $Price_{Grid}$ denote the electricity generation cost by wind turbine unit, micro-turbine unit, photovoltaic panel, battery storage unit, MCAES unit, and the market clearing price of the electricity market at the purported time interval in $.

3.2. Emission cost

The estimation of emission and environmental cost and inclusion of it in the objective function of electricity generation is a crucial step toward more real optimization of prices and costs and clarification in actual pricing, which justifies the assessment and inclusion of emission parameters in power system operation modeling. This matter facilitates the acceptability of the utilization of renewable resources which incline the power systems to environmental and economic sustainability in the long-term. In this study, in order to model the emission, the most prevalent pollutant caused by power systems such as NO_x, CO_2, and SO_2 are taken into account [40]. Eqs. (44) and (45) show the costs pertaining to emission as well as the corresponding objective function.

$$\begin{aligned} \mathrm{C}_{Emission} &= \alpha_{CO_2}\left(P_{MT}(t) \times E_{MT}^{CO_2}(t) + P_{MCAES}(t) \times E_{MCAES}^{CO_2}(t)\right) \\ &+ \alpha_{SO_2}\left(P_{MT}(t) \times E_{MT}^{SO_2}(t) + P_{MCAES}(t) \times E_{MCAES}^{SO_2}(t)\right) \\ &+ \alpha_{NO_X}\left(P_{MT}(t) \times E_{MT}^{NO_X}(t) + P_{MCAES}(t) \times E_{MCAES}^{NO_X}(t)\right) \end{aligned} \quad (44)$$

$$f_2 = Min \sum_{t=1}^{N_t} \mathrm{C}_{Emission} \quad (45)$$

3.3. The energy not supplied (ENS) cost and excess generation cost

In order to avoid load shedding and forced outage of generation units, virtual costs are defined for unsupplied power ($C_{UN,t}$) and excess generation ($C_{EX,t}$). In this paper, the corresponding price with the mentioned costs is supposed to be equal to 2 $/kWh [41]. Hence, the objective function associated with unsupplied cost and excess generation cost can be proposed by Eq. (46):

$$f_3 = Min\sum_{t=1}^{N_t} C_{UN,t} + C_{EX,t} \quad (46)$$

The proposed strategy for energy management is subjected to diminish the generation cost as well as emission and unsupplied power. The objective function is composed of summation of each individual operation cost of battery and MCAES (which operate in two modes of charging and discharging), the emission cost, the unsupplied energy cost, and the cost of provision of excess power. Thus, the final objective function of the problem is modeled by Eq. (47), which has to be minimized.

$$f = min\sum_{t=1}^{24}\{f_1 + f_2 + f_3\} \quad (47)$$

3.4. System constraints

The suggested objective function has to be minimized subject to satisfy the following constraints:

A. The power balance equation; The summation of generated power in the network must be equal to total consumed power. This constraint is expressed in Eq. (48). It is noticeable that the considered demand in this equation is replaced with the demand resulted from demand response implication.

$$P_t^{wind} + P_t^{PV} + P_t^{MT} + P_t^{B,disc} + P_t^{MCAES,disc} + P_{UN,t} = Load(t) + P_t^{B,charge} + P_t^{MCAES,charge} + P_{EX,t} \quad (48)$$

B. The constraints associated with the wind turbine, solar cells, and micro-turbine

C. The technical constraints of the battery storage facility

D. The technical constraints of MCAES facility

E. The constraints associated with DRPs

4. Teaching-learning-based optimization algorithm (TLBO)

The basis of the procedure of TLBO is inspired by the teaching of a teacher in a classroom. The quality of learning by the students highly depends on the quality of teaching. In addition, the review of newly learned items by each individual student can effectively improve the learning procedure. This idea is the basis of the TLBO algorithm. The TLBO consists of two main phases. The first corresponds with the impact of the teacher in the learning mechanism. The second is associated with the impact of review and interactive learning by the students of the class. The pseudo-code of the TLBO optimization algorithm is described in the Fig. 6.

4.1. Teacher phase

A good teacher is that one, who tries to improve to upgrade the knowledge level of the class to their own knowledge level. In practice, the knowledge level of students cannot reach the level of their own teacher, but it can approximate to that level. The grade of proximity depends on the learning ability of the class. This matter is represented by Eq. (49), as shown below:

$$\overline{X}_{diff}^{k} = rand() \times \left(T^k - R_t \times M^k\right) \quad (49)$$

In the above equation, T^k denotes the teacher at the t^{th} iteration, M^k shows the mean of the class at the t^{th} iteration. R^t is the teaching factor that can take the value of 0 or 1, and its value derived randomly from a specific distribution at each iteration. The population at the next iteration is created according to Eq. (50):

$$\overline{X}_{new}^{k+1} = \overline{X}_{old}^{k} + \overline{X}_{diff}^{k} \quad (50)$$

In the above equation, $\overline{X}_{old}^{k}$ is the member of the set at the last iteration and $\overline{X}_{new}^{k+1}$ shows the member of the set at the current iteration. A cost function is dedicated to the new member of the set. The value of the cost function in the current iteration is compared with the value at the last iteration. If the new obtained value is lower than the old value, the new member must be replaced with the old one.

```
For i =1 to D
    a← select a random integer in {1, 2, ..., NP}
    M(i) = X^a(i);
End
For k=1 to NP
    IF r1 < 0.5 // Teaching
        For i = 1 to D
            IF r2 < SP
                TF(i) = round (1 + r2);
                X^new(i)= X^k(i) + r3×(X^best(i) – TF(i)×M(i));
            End
        End For
    Else // Learning each other between learns
        For i = 1 to D
            IF < SP
                r←select a random integer in {1, 2, ..., NP}
                If X^r is better than X^k
                    X^new(i)= X^k(i) + r4×(X^r(i) – X^k(i));
                Else
                    X^new(i)= X^k(i) + r5×(X^k(i) – X^r(i));
                End
            End If
    End
End
If X^new is better than X^k
    X^k = X^new,
End
    where, r1, r2, r3, r4 and r5 are uniformly distributed random
numbers between 0 and 1
```

Fig. 6. The pseudocode of TLBO algorithm

4.2. Student phase

The students can improve their own knowledge level in two ways. They can attend the class and learn through their teacher. They can also review the course by themselves or having interactive reviews by other students. To model this fact, it is supposed that each student can randomly have a discussion with another student. The corresponding mathematical model is expressed in Eq. (51).

$$\overline{X}_{new} = \overline{X}_{old} + rand() \times \left(\overline{X}_i - \overline{X}_j\right) \quad (51)$$

Where, $\overline{X}_i$ and $\overline{X}_j$ are the i^{th} and j^{th} members (students). $\overline{X}_{old}$ and $\overline{X}_{new}$ are the old and new members of the population set respectively. After generation and conducting initial calculations relevant to the new member of the set, its cost function value must be compared with the corresponding value for that member in the last iteration. If the new obtained value is lower than the previous, the new

member is replaced with the last one. This procedure must be repeated for a certain number of iterations. The paradigm of the TLBO algorithm is demonstrated in Fig. 7. Further information can be found in [42-43].

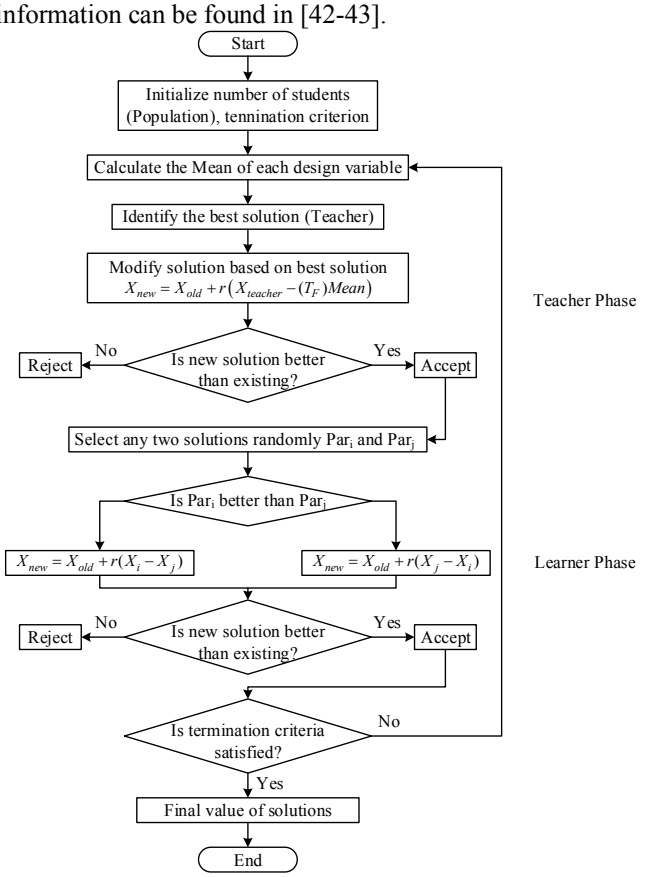

Fig. 7. The flowchart of TLBO algorithm

5. Simulation and numerical analysis

In the following section, in order to evaluate the performance of the proposed strategy, a simulation of a microgrid including micro-turbine, wind turbine, solar panel, battery, and MCAES system is carried out. In addition, the impact of DRPs on the consumption behavior of purported microgrid's loads along with its implications on corresponding prices are investigated. Finally, various operation scenarios are compared to each other, and the effectiveness of the model is assessed. Hence, four scenarios are introduced as follows:

- Scenario 1: The microgrid's required energy is supplied only by non-renewable sources.
- Scenario 2: The microgrid's required energy is supplied by both renewable and non-renewable sources. (without the presence of storage units)
- Scenario 3: The microgrid's required energy is supplied by both renewable and non-renewable sources while storage units are integrated into the microgrid's model.
- Scenario 4: The microgrid's required energy is supplied by both renewable and non-renewable sources in the presence of storage units and with the incorporation of DRPs.

5.1. Input data

As it is illustrated in Fig. 1, the targeted microgrid as a case study includes various sources such as micro-turbine, wind turbine, solar panel, battery, and MCAES unit. Figs. 8 and 9 show the electric demand curve and the maximum generated power by wind and solar sources within various hours of the considered day. In order to calculate the generated power of wind and photovoltaic units, the databases of mean wind speed records and solar radiation records of a 24-hour period in September corresponded with the Yazd city, located in Iran, are employed. The technical characteristics of integrated resources, as well as the deployed energy storage facilities, are shown in Table 1.

Table 1. The characteristics of integrated power sources into the microgrid

Unit	MT	WT	PV	Battery	M-CAES
P_{min} (kW)	200	0	0	-45	-500
P_{max} (kW)	3000	660	1000	45	500
SUC & SDC ($)	1.1227	0	0	0	0.2975
Bid ($/kWh)	0.0181	0.025	0.025	0.0223	0.0223
CO_2 (kg/MWh)	720	0	0	10	126.6
SO_2 (kg/MWh)	0.0054	0	0	0.0002	0.00095
NO_x (kg/MWh)	0.23	0	0	0.001	0.04

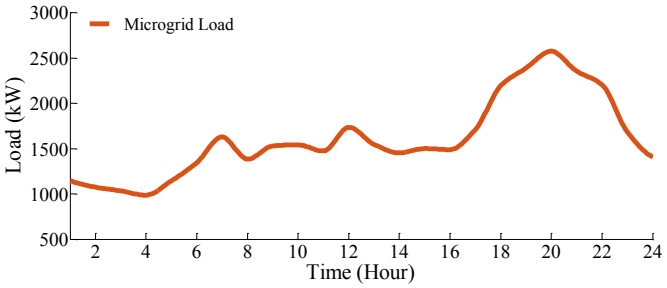

Fig. 8. The electrical demand curve of the microgrid's loads

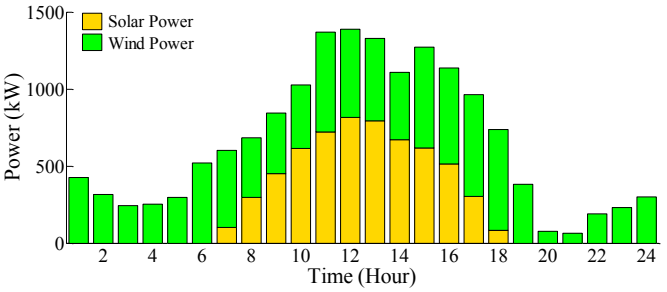

Fig. 9. Maximum generation of wind and photovoltaic units

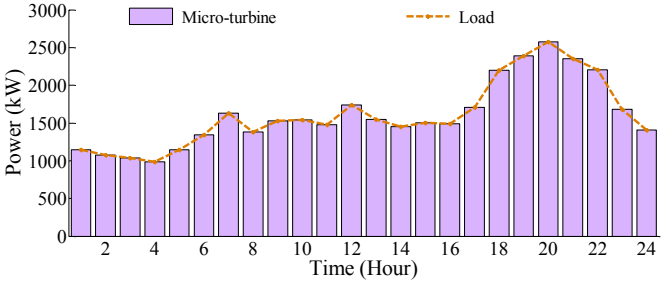

Fig. 10. The commitment state and generated power of micro-turbine unit in the first scenario

5.2. Scenario 1

In the first scenario, the short-term scheduling problem for the microgrid is surveyed regardless of the presence of renewable sources as well as storage facilities and without

the integration of DRPs into the model. In this case, the total energy demand is supplied by the micro-turbine unit. Fig. 10 demonstrates the commitment state and generation of the micro-turbine unit within the time horizon of the study in scenario 1.

In this scenario, the micro-turbine unit must generate 38553.32 kW of electrical energy. In order to generate this amount of active power, the micro-turbine unit requires to consume 463.627 m^3 of fuel. In this study, the cost of each cubic meter of fuel is supposed to be equal with 0.1 $/$m^3$. Therefore, the generation cost of micro-turbine, which is composed of fuel cost, start-up and shutdown costs, and maintenance cost, will be equal with $698.803. The generation of this amount of power entails the emission of 8952.357 kg of CO_2, 30.136 kg of CO, 3.338 kg of unburned hydrocarbon (UHCs), 23.621 kg of SO_2, and 268.903 kg of NO_x. The emission of this amount of air pollution incurs the cost of $365.168. The cost of energy not supplied and excess generation is $0.617. The total operation cost of the system in this scenario, including emission cost and energy not supplied cost is about $1064.588, which conveys the average operation cost of 0.0276 $/kWh.

5.3. Scenario 2

In the second scenario, the targeted microgrid is supplied by wind, solar, and micro-turbine units. Fig. 11 depicts the commitment state and generation dispatch between these units in various hours.

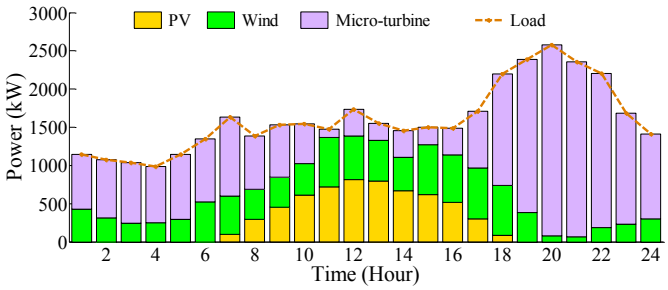

Fig. 11. The commitment state and the load dispatch of between generating units in scenario 2

With respect to the problem's objective function, the wind unit and the photovoltaic plant have the most generation contribution in the satisfaction of microgrid's demand by 9774.787 kW and 5988.295 kW, respectively. In this case, the wind unit and photovoltaic unit will have a revenue of $244.369 and $149.707, respectively, from the source of sale of electricity to the grid. In this schedule, the micro-turbine unit must generate 22790.238 kW of power, which is the most contribution in meeting demand among these three types of generating units. The fuel consumption of micro-turbine in this scenario is about 2740.663 m^3 that implies a reduction in comparison with the previous scenario. The overall operating cost of the micro-turbine is $413.087. The cost relevant to the emission is estimated to be $210.243 (5148.481 kg_{CO2}, 17.351 kg_{CO}, 1.922 kg_{UHCs}, 13.600 kg_{SO2}, and 154.819 kg_{NOx}). The energy not supplied cost and excess generation cost is risen compared with scenario 1 and reached to $0.673. The total operation cost of the system in this scenario is $1018.081, while the emission cost, energy not supplied cost, and excess generation cost are taken into account. Thus, the average operation cost is 0.0264 $/kWh.

5.4. Scenario 3

Nowadays, the development of energy storage technologies for emergency power provision has gained more importance. Besides, due to intermittency in power systems, the deployment of energy storage technologies for in the electrical grids is a vital element in restructuring for increasing the penetration of renewable sources and integration of distributed generation as well as improvement of power quality and alleviation of environmental issues. In this scenario, the impact of the integration of energy storage facilities in the operation model of the microgrid is investigated. Fig. 12 demonstrates the commitment and dispatch of power among generation sources in scenario 3.

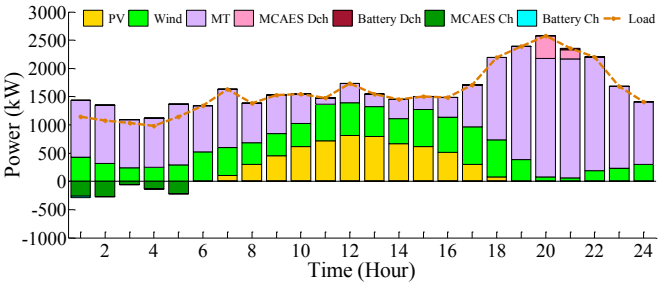

Fig. 12. The unit commitment and generation dispatch of units in scenario 3

As can be seen from Fig. 12, the MCAES unit should store energy within 1 to 5 o'clock, as the demand of the microgrid is low. In contrast, this unit should deliver this power back to the grid (discharge) at 20 and 21 o'clock, while the electrical demand of the microgrid will reach a peak. In this case, the MCAES unit has received a profit of $2.364 from the source of sale of power to the microgrid. Likewise, the battery storage unit stores energy at 1 o'clock and discharge it at 21 o'clock. The battery unit earns a profit of $0.0973, meanwhile. The wind and photovoltaic systems receive similar profitability as scenario 2 for the same generation. The generation of the micro-turbine unit is decreased in comparison with the previous scenario, and it should generate 22411.989 kW. Consequently, the amount of fuel consumption and the generation cost of this unit are mitigated to 2695.176 m^3 and $406.231. The generation of this amount of power by micro-turbine unit entails the emission of 4886.354 kg_{CO2}, 16.466 kg_{CO}, 1.823 kg_{UHCs}, 12.907 kg_{SO2}, and 146.937 kg_{NOx}. The emission of such amount of pollutants incurs the emission cost of $199.538. The summation of energy not supplied cost and excess generation cost is risen compared with scenario 2 and reached $0.758. Thus, the total operation cost of the system and the demand provision cots per kWh are $1003.065 and $0.026, respectively. Hence, it can be declared that the energy storage systems not only can supply the demand, but also can have positive impacts on the improvement of frequency, voltage, peak shaving management, and increase the penetration of renewable sources, mitigation of operation cost of grids, and consequently the reduction of total operation cost of electricity.

5.5. Scenario 4

In general, the main goal of DRPs is to alleviate electricity consumption in critical and peak hours. The critical hours are defined as the time when the price of the wholesale market is spiked, or the reserve level of the grid is extremely decreased due to a contingency such as a fault on a transmission line, or a generator, or due to dreadful weather. In this scenario, a time-based rate DRP is incorporated. The aim of this program is to shift energy consumption from peak to off-peak hours. Fig. 13 shows the demand curve of the microgrid before and after the execution of the targeted DRP. The unit commitment and generation dispatch of distributed generation sources as well as storage units, according to scenario 4, is demonstrated in Fig. 14.

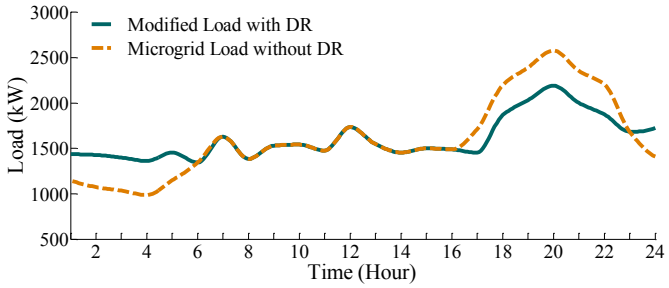

Fig. 13. Demand curve of the microgrid before and after implementation of DRP

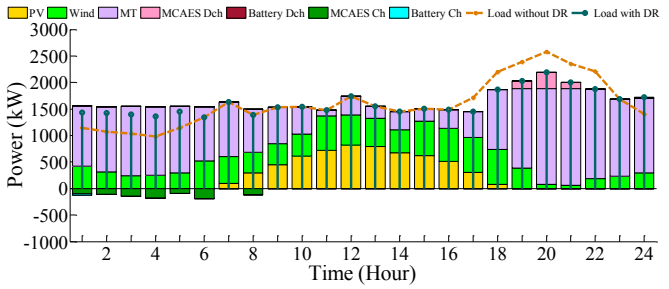

Fig. 14. The unit commitment and generation dispatch of units in scenario 4

The wind and solar units have the same profitability as scenarios 2 and 3 by selling power to the microgrid. In comparison with scenario 3, the micro-turbine unit should generate at a lower level by 22401.567 kW. Hence, the generation cost of micro-turbine and the fuel consumption of this unit has decreased to \$406.042 and 2693.923 m^3. As a consequence, the emission cost of the microgrid reached to \$190.908 due to the emission of 4675.015 kg_{CO2}, 15.756 kg_{CO}, 1.747 kg_{UHCs}, 12.349 kg_{SO2}, and 140.581 kg_{NOx}. The battery storage is scheduled to charge at 1 o'clock while it should discharge at 24 o'clock. This measure procures a profit of \$0.0972 for this unit. Besides, the MCAES unit stores power from hours 1 to 6 and 8 o'clock, and it should discharge from 19 to 21 o'clock. The profit of MCAES unit, similar to the third scenario, is about \$0.722. The revenue of participant loads in DRP is estimated to be about \$1.303. Therefore, the total operation cost and the mean operation cost per kWh in scenario 4 are \$995.514 and \$0.0258. As can easily be perceived, in the fourth scenario, the implementation of DRP underlies the tangible reduction of generation cost, the final electricity price, and emission of air pollutants. Therefore, it can be concluded that the integrated operation of generation sources along with storage facilities and DRPs can be led to the reduction of generation cost, alleviation of environmental pollutants, and improvement of reliability indices. The operation cost includes generation cost, emission cost, energy not supplied cost, and excess generation cost. In order to have better comprehension, the variation of operation cost in scenario 4 is depicted in Fig. 15 for a 24-hour period.

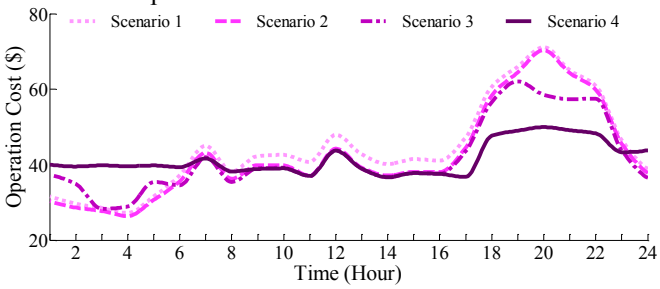

Fig. 15. The operation cost of the microgrid for a daily time horizon

6. Conclusions

In recent years, the concept of microgrid has been comprehensively investigated in combination with crucial topics such as optimized operation management and scheduling, distribution system planning, reliability, and controlling issues. The microgrid concept is a broad topic with a diverse set of challenging issues. There are intriguing ideas in the area of microgrid research. One of the most salient topics and challenges of microgrids is the procedure of management and scheduling of renewable resources and other generation sources of energy for a secure and reliable power supply. In this paper, this problem is introduced as an optimization problem with three different objectives, in which the generation cost of the microgrid, the emission of fossil-burning units, and the costs pertaining to energy not supplied and excess generation are integrated into the model. In order to reach an inspired performance, it is assumed that demand-side loads can participate actively and elastically in demand response programs. The main outcomes of this research can be summarized as follows:

1. The proposed model not only has a simple structure but also has high capability in reaching optimal results.

2. The incorporation of a multi-objective function in the optimization problem procures manoeuvring points and facilitates the implementation of different scenarios. Thus, in order to boost a certain objective, the most appropriate scenario can be maintained for the arrangement of generation dispatch scheduling.

3. In the conducted modelling of the fourth scenario, the results imply that the integrated operation of all generation sources, as well as storage facilities along with the implementation of demand response programs, has been resulted in substantial mitigation of generation cost and final electricity price, and remarkable reduction of emission of air pollutants.

References

[1] Shahinzadeh, H., Fathi, S.H. and Hasanalizadeh-Khosroshahi, A., 2016, April. Long-term energy planning in IRAN using LEAP scenario: Using combined heat and power (CHP). In *2016 Iranian*

Conference on Renewable Energy & Distributed Generation (ICREDG) (pp. 32-37). IEEE.

[2] Adefarati, T. and Bansal, R.C., 2019. Reliability, economic and environmental analysis of a microgrid system in the presence of renewable energy resources. *Applied Energy*, *236*, pp.1089-1114.

[3] Muttaqi, K.M., Le, A.D., Aghaei, J., Mahboubi-Moghaddam, E., Negnevitsky, M. and Ledwich, G., 2016. Optimizing distributed generation parameters through economic feasibility assessment. *Applied energy*, *165*, pp.893-903.

[4] Hadayeghparast, S., Farsangi, A.S., Shayanfar, H. and Karimipour, H., 2019, May. Stochastic Multi-Objective Economic/Emission Energy Management of a Microgrid in Presence of Combined Heat and Power Systems. In *2019 IEEE/IAS 55th Industrial and Commercial Power Systems Technical Conference (I&CPS)* (pp. 1-9). IEEE.

[5] Shahinzadeh, H., Gheiratmand, A., Fathi, S.H. and Moradi, J., 2016, April. Optimal design and management of isolated hybrid renewable energy system (WT/PV/ORES). In *2016 21st Conference on Electrical Power Distribution Networks Conference (EPDC)* (pp. 208-215). IEEE.

[6] Bornapour, M., Hooshmand, R.A., Khodabakhshian, A. and Parastegari, M., 2017. Optimal stochastic coordinated scheduling of proton exchange membrane fuel cell-combined heat and power, wind and photovoltaic units in micro grids considering hydrogen storage. *Applied energy*, *202*, pp.308-322.

[7] Hosseini, S.J.A.D., Moradian, M., Shahinzadeh, H. and Ahmadi, S., 2018. Optimal Placement of Distributed Generators with Regard to Reliability Assessment using Virus Colony Search Algorithm. *International Journal of Renewable Energy Research (IJRER)*, *8*(2), pp.714-723.

[8] Dorahaki, S., Rashidinejad, M., Mollahassani-pour, M. and Bakhshai, A., 2019. An efficient hybrid structure to solve economic-environmental energy scheduling integrated with demand side management programs. *Electrical Engineering*, pp.1-12.

[9] Nazari-Heris, M., Mohammadi-Ivatloo, B., Gharehpetian, G.B. and Shahidehpour, M., 2018. Robust short-term scheduling of integrated heat and power microgrids. *IEEE Systems Journal*.

[10] Talapur, G.G., Suryawanshi, H.M., Xu, L. and Shitole, A.B., 2018. A reliable microgrid with seamless transition between grid connected and islanded mode for residential community with enhanced power quality. *IEEE Transactions on Industry Applications*, *54*(5), pp.5246-5255.

[11] Llanos, J., Olivares, D.E., Simpson-Porco, J.W., Kazerani, M. and Sáez, D., 2019. A novel distributed control strategy for optimal dispatch of isolated microgrids considering congestion. *IEEE Transactions on Smart Grid*.

[12] Aryanpur, V., Atabaki, M.S., Marzband, M., Siano, P. and Ghayoumi, K., 2019. An overview of energy planning in Iran and transition pathways towards sustainable electricity supply sector. *Renewable and Sustainable Energy Reviews*, *112*, pp.58-74.

[13] Anastasiadis, A.G., Konstantinopoulos, S., Kondylis, G.P. and Vokas, G.A., 2017. Electric vehicle charging in stochastic smart microgrid operation with fuel cell and RES units. *International Journal of Hydrogen Energy*, *42*(12), pp.8242-8254.

[14] Trevathan-Tackett, S.M., Wessel, C., Cebrián, J., Ralph, P.J., Masqué, P. and Macreadie, P.I., 2018. Effects of small-scale, shading-induced seagrass loss on blue carbon storage: Implications for management of degraded seagrass ecosystems. *Journal of applied ecology*, *55*(3), pp.1351-1359.

[15] Balali, M.H., Nouri, N., Nasiri, A. and Seifoddini, H., 2015, November. Development of an economical model for a hybrid system of grid, PV and Energy Storage Systems. In *2015 International Conference on Renewable Energy Research and Applications (ICRERA)* (pp. 1108-1113). IEEE.

[16] Ghalelou, A.N., Fakhri, A.P., Nojavan, S., Majidi, M. and Hatami, H., 2016. A stochastic self-scheduling program for compressed air energy storage (CAES) of renewable energy sources (RESs) based on a demand response mechanism. *Energy conversion and management*, *120*, pp.388-396.

[17] Moradi, J., Shahinzadeh, H., Khandan, A. and Moazzami, M., 2017. A profitability investigation into the collaborative operation of wind and underwater compressed air energy storage units in the spot market. *Energy*, *141*, pp.1779-1794.

[18] Simorgh, H., Doagou-Mojarrad, H., Razmi, H. and Gharehpetian, G.B., 2017. Cost-based optimal siting and sizing of electric vehicle charging stations considering demand response programmes. *IET Generation, Transmission & Distribution*, *12*(8), pp.1712-1720.

[19] Imani, M.H., Niknejad, P. and Barzegaran, M.R., 2019. Implementing Time-of-Use Demand Response Program in microgrid considering energy storage unit participation and different capacities of installed wind power. *Electric Power Systems Research*, *175*, p.105916.

[20] Jadidbonab, M., Dolatabadi, A., Mohammadi-Ivatloo, B., Abapour, M. and Asadi, S., 2019. Risk-constrained energy management of PV integrated smart energy hub in the presence of demand response program and compressed air energy storage. *IET Renewable Power Generation*, *13*(6), pp.998-1008.

[21] Zheng, Y., Jenkins, B.M., Kornbluth, K. and Træholt, C., 2018. Optimization under uncertainty of a biomass-integrated renewable energy microgrid with energy storage. *Renewable energy*, *123*, pp.204-217.

[22] Mercado, K.D., Jiménez, J. and Quintero, M.C.G., 2016, November. Hybrid renewable energy system based on intelligent optimization techniques. In *2016 IEEE International Conference on Renewable Energy Research and Applications (ICRERA)* (pp. 661-666). IEEE.

[23] Shahinzadeh, H., Gheiratmand, A., Moradi, J. and Fathi, S.H., 2016, April. Simultaneous operation of near-to-sea and off-shore wind farms with ocean renewable energy storage. In *2016 Iranian Conference on Renewable Energy & Distributed Generation (ICREDG)* (pp. 38-44). IEEE.

[24] Munkhammar, J., Widén, J. and Rydén, J., 2015. On a probability distribution model combining household power consumption, electric vehicle home-charging and photovoltaic power production. *Applied Energy*, *142*, pp.135-143.

[25] Shepero, M., Munkhammar, J., Widén, J., Bishop, J.D. and Boström, T., 2018. Modeling of photovoltaic power generation and electric vehicles charging on city-scale: A review. *Renewable and Sustainable Energy Reviews*, *89*, pp.61-71.

[26] Shayanfar, H.A., Shayeghi, H. and Bagherzadeh, L., Optimal Allocation of Electric Vehicle Parking Lots for Improving the Efficiency of Distribution System. In *2019 Int'l Conf. Artificial Intelligence (ICAI'19)* (pp. 116-122). CSREA Press.

[27] Boland, J. and Grantham, A., 2018. Nonparametric Conditional Heteroscedastic Hourly Probabilistic Forecasting of Solar Radiation. *J*, *1*(1), pp.174-191.

[28] Alzahrani, A., Shamsi, P., Ferdowsi, M. and Dagli, C., 2017, November. Solar irradiance forecasting using deep recurrent neural networks. In *2017 IEEE 6th international conference on renewable energy research and applications (ICRERA)* (pp. 988-994). IEEE.

[29] Shahinzadeh, H., Moradi, J., Gharehpetian, G.B., Fathi, S.H. and Abedi, M., 2018, November. Green Power Island, a Blue Battery Concept for Energy Management of High Penetration of Renewable Energy Sources with Techno-Economic and Environmental Considerations. In *2018 Smart Grid Conference (SGC)* (pp. 1-9). IEEE.

[30] Bagherzadeh, L. and Shayeghi, H. and SeyedShenava, SJ., 2019, June. Optimal Allocation of Electric Vehicle Parking lots and Renewable Energy Sources Simultaneously for Improving the Performance of Distribution System. In *2019 24th Electrical Power Distribution Conference (EPDC)* (pp. 87-94). IEEE.

[31] Shahinzadeh, H., Moradi, J., Gharehpetian, G.B., Abedi, M. and Hosseinian, S.H., 2018, November. Multi-Objective Scheduling of CHP-Based Microgrids with Cooperation of Thermal and Electrical Storage Units in Restructured Environment. In *2018 Smart Grid Conference (SGC)* (pp. 1-10). IEEE.

[32] Kerdphol, T., Fuji, K., Mitani, Y., Watanabe, M. and Qudaih, Y., 2016. Optimization of a battery energy storage system using particle swarm optimization for stand-alone microgrids. *International Journal of Electrical Power & Energy Systems*, *81*, pp.32-39.

[33] Yang, Y., Bremner, S., Menictas, C. and Kay, M., 2018. Battery energy storage system size determination in renewable energy systems: A review. *Renewable and Sustainable Energy Reviews*, *91*, pp.109-125.

[34] Shahinzadeh, H., Moazzami, M., Fathi, S.H. and Gharehpetian, G.B., 2016, December. Optimal sizing and energy management of a grid-connected microgrid using HOMER software. In *2016 Smart Grids Conference (SGC)* (pp. 1-6). IEEE.

[35] Kim, Y.M., Lee, J.H., Kim, S.J. and Favrat, D., 2012. Potential and evolution of compressed air energy storage: energy and exergy analyses. *Entropy*, *14*(8), pp.1501-1521.

[36] Karellas, S. and Tzouganatos, N., 2014. Comparison of the performance of compressed-air and hydrogen energy storage systems: Karpathos island case study. *Renewable and Sustainable Energy Reviews*, *29*, pp.865-882.

[37] Aalami, H.A., Moghaddam, M.P. and Yousefi, G.R., 2015. Evaluation of nonlinear models for time-based rates demand response programs. *International Journal of Electrical Power & Energy Systems*, *65*, pp.282-290.

[38] UESHIMA, M., YUASA, K. and BABASAKI, T., 2018, October. Improving Energy Self-Consumption Rate in Renewable Energy System A study using a robust optimization method considering uncertainty of power generation. In *2018 7th International Conference on Renewable Energy Research and Applications (ICRERA)* (pp. 281-286). IEEE.

[39] Sehar, F., Pipattanasomporn, M. and Rahman, S., 2016. An energy management model to study energy and peak power savings from PV and storage in demand responsive buildings. *Applied energy*, *173*, pp.406-417.

[40] Shahinzadeh, H., Moradi, J., Gharehpetian, G.B., Fathi, S.H. and Abedi, M., 2018, November. Optimal Energy Scheduling for a Microgrid Encompassing DRRs and Energy Hub Paradigm Subject to Alleviate Emission and Operational Costs. In *2018 Smart Grid Conference (SGC)* (pp. 1-10). IEEE.

[41] Alvarez, S.R., Ruiz, A.M. and Oviedo, J.E., 2017, November. Optimal design of a diesel-PV-wind system with batteries and hydro pumped storage in a Colombian community. In *2017 IEEE 6th International Conference on Renewable Energy Research and Applications (ICRERA)* (pp. 234-239). IEEE.

[42] Rao, R.V., 2016. Teaching-learning-based optimization algorithm. In *Teaching learning based optimization algorithm* (pp. 9-39). Springer, Cham.

[43] Kaveh, A. and Bakhshpoori, T., 2019. *Metaheuristics: Outlines, MATLAB Codes and Examples*. Springer International Publishing.